AGU PUBLICATIONS

Geophysical Research Letters

RESEARCH LETTER
10.1002/2016GL069643

Special Section:
First results from NASA's Magnetospheric Multiscale (MMS) Mission

A telescopic and microscopic examination of acceleration in the June 2015 geomagnetic storm: Magnetospheric Multiscale and Van Allen Probes study of substorm particle injection

D. N. Baker[1], A. N. Jaynes[1], D. L. Turner[2], R. Nakamura[3], D. Schmid[4], B. H. Mauk[5], I. J. Cohen[5], J. F. Fennell[6], J. B. Blake[6], R. J. Strangeway[7], C. T. Russell[8], R. B. Torbert[9], J. C. Dorelli[10], D. J. Gershman[11], B. L. Giles[11], and J. L. Burch[12]

[1]Laboratory for Atmospheric and Space Physics, University of Colorado Boulder, Boulder, Colorado, USA, [2]Space Sciences Department, The Aerospace Corporation, Los Angeles, California, USA, [3]Space Research Institute OEAW, Space Research Institute, Austrian Academy of Sciences, Graz, Austria, [4]Space Research Institute Graz, Graz, Austria, [5]Johns Hopkins University Applied Physics Laboratory, Laurel, Maryland, USA, [6]The Aerospace Corporation, Los Angeles, California, USA, [7]Institute of Geophysics and Planetary Physics, University of California, Los Angeles, California, USA, [8]Institute of Geophysics and Planetary Physics, University of California, Los Angeles, California, USA, [9]Space Science Center, University of New Hampshire, Durham, New Hampshire, USA, [10]NASA/GSFC, Greenbelt, Maryland, USA, [11]NASA Goddard Space Flight Center, Greenbelt, Maryland, USA, [12]Southwest Research Institute, San Antonio, Texas, USA

Key Points:
- New MMS data show that magnetic reconnection is a fundamental component of relativistic particle acceleration in Earth's magnetosphere
- The composition and timing of substorm injection fronts that supply radiation belt seed particles can be well resolved using MMS
- Combined RBSP and MMS data demonstrate that magnetospheric substorms are an essential element in the near-Earth radiation belt system

Supporting Information:
- Figure S1
- Figure S2
- Supporting Information S1

Correspondence to:
D. N. Baker,
daniel.baker@lasp.colorado.edu

Citation:
Baker, D. N., et al. (2016), A telescopic and microscopic examination of acceleration in the June 2015 geomagnetic storm: Magnetospheric Multiscale and Van Allen Probes study of substorm particle injection, *Geophys. Res. Lett.*, *43*, 6051–6059, doi:10.1002/2016GL069643.

Received 18 MAY 2016
Accepted 2 JUN 2016
Accepted article online 7 JUN 2016
Published online 29 JUN 2016

Abstract An active storm period in June 2015 showed that particle injection events seen sequentially by the four (Magnetospheric Multiscale) MMS spacecraft subsequently fed the enhancement of the outer radiation belt observed by Van Allen Probes mission sensors. Several episodes of significant southward interplanetary magnetic field along with a period of high solar wind speed ($V_{sw} \gtrsim 500$ km/s) on 22 June occurred following strong interplanetary shock wave impacts on the magnetosphere. Key events on 22 June 2015 show that the magnetosphere progressed through a sequence of energy-loading and stress-developing states until the entire system suddenly reconfigured at 19:32 UT. Energetic electrons, plasma, and magnetic fields measured by the four MMS spacecraft revealed clear dipolarization front characteristics. It was seen that magnetospheric substorm activity provided a "seed" electron population as observed by MMS particle sensors as multiple injections and related enhancements in electron flux.

1. Introduction

The International Solar Terrestrial Physics (ISTP) program was a coordinated spacecraft project that allowed broad observation of the connected Sun-Earth system [e.g., *Acuña et al.*, 1995]. ISTP mission elements—some of which are still operating today—permitted monitoring of the Sun's activity on the one hand and detection near the Earth of significant solar wind disturbances on the other hand. This gave a broad "telescopic" view of the global system behavior, while the four-spacecraft Cluster constellation permitted a "microscope" perspective of key regions in order to understand detailed properties of the dynamic magnetospheric system. This telescope-microscope concept proved to be of great benefit in general as well as in specific studies of complex phenomena such as magnetospheric substorms [*Baker et al.*, 2002].

Prior published results from several spacecraft missions have shown general patterns of substorm activity in the plasma sheet, including localized plasma transport, bursty bulk flows, and sharp energetic particle injections into geostationary orbit or even closer to the Earth [*Angelopoulos et al.*, 1992; *Baker et al.*, 1996; *Reeves et al.*, 1996; *Sergeev et al.*, 1998; *Birn et al.*, 1998]. More recent studies have examined closely the relationships between bursty bulk flows and so-called dipolarization fronts [*Runov et al.*, 2011]. Localized dipolarizing flux bundles [*Liu et al.*, 2014, 2016], for example, are thought to be composed of reconnected plasma flux tubes traveling earthward, which have dipolarization fronts at their leading edge. Comprehensive statistical studies [e.g., *Gabrielse et al.*, 2014] have demonstrated spatial and temporal relationships between energetic particle injections and dipolarization fronts in the near-Earth plasma sheet. The underlying mechanisms of magnetospheric particle acceleration and the relation of particle injections to substorms have been reviewed by *Birn et al.* [2012].

A new chapter in microscopic observing capabilities for energetic particle injections has been opened with the launch of the Magnetospheric Multiscale (MMS) mission in March 2015 [*Burch et al.*, 2015]. The four-satellite

MMS constellation is capable of unprecedented spatial and temporal resolution examination of plasma physical properties in Earth's neighborhood [e.g., *Burch et al*., 2016]. When MMS observations are carried out in conjunction with other elements of the modern-day Heliophysics System Observatory [*National Research Council*, 2013], a greatly extended possibility exists to use the telescope-microscope approach to advance space plasma research.

In the present study, we examine a substorm event during one of the strongest geomagnetic storms of the last decade [see, e.g., *Baker et al*., 2016]. This storm was the result of an active region on the Sun that produced numerous coronal mass ejections and associated interplanetary shock waves in June 2015. The solar storms initiated distinct magnetospheric responses that were well observed both by the MMS spacecraft (in their instrument "commissioning" phases during this time) as well as the Van Allen Probes spacecraft [*Mauk et al*., 2012] that provided broad context for magnetospheric and radiation belt behavior during this storm interval. We report here on a particularly well observed substorm injection sequence that allows us to use the unique MMS temporal and spatial detection abilities.

2. Overview of the June 2015 Storm Period

Figure 1 shows the trajectory of the MMS spacecraft for a period on 21–22 June 2015 (Figure 1a). This panel also shows the orbits for the Van Allen Probes spacecraft A and B for the same period. Figure 1 also shows the auroral electrojet (*AE*) index values from 15 June to 5 July of 2015 (Figure 1c) and the storm time ring current (*SYM-H*) index (Figure 1b) for the same interval. The powerful geomagnetic storm initiated on 21 June is evident in the *SYM-H* index data. The storm reached a peak strength of *SYM-H* = −207 nT early on 23 June.

Given the orbital location of the MMS constellation (Figure 1a) during this time, the satellite instruments would be expected to effectively detect magnetospheric particle injection events in the premidnight sector, especially when the MMS spacecraft were near apogee or on their inbound trajectory legs. From the relative locations of the Van Allen Probes (VAP) orbits, radial alignments with the MMS spacecraft were expected to be possible for at least some periods of time during this storm.

A detailed display of solar wind, interplanetary magnetic field (IMF), and geomagnetic data for the period of 00:00 UT on 22 June through 24:00 UT on 23 June 2015 is shown in Figures 1d–1i. Activity was initiated with the arrival of an interplanetary shock wave at ~05:30 UT on 22 June. The largest solar wind disturbances for this time period occurred at 18:36 UT on 22 June, noted in Figure 1. A major solar wind density and dynamic pressure pulse was recorded at that time, and the solar wind speed concurrently jumped up to >700 km/s. This caused a substantial further increase in *AE* activity, and *SYM-H* exhibited a large additional depression following the 18:36 UT shock arrival.

3. Shock and Substorm Signatures at MMS

As may be seen from Figure 1a orbital plots, the MMS constellation was on its outbound leg in the premidnight sector on 22 June when the interplanetary shock wave struck the magnetosphere. Figure 2 shows the Fast Plasma Investigation (FPI) electron data (Figure 2a), Energetic Ion Spectrometer (EIS) electron data (Figure 2c), and Flux Gate Magnetometer (FGM) magnetic field data (Figure 2b) for the period of 18:00–21:00 UT on 22 June 2015. The data shown are only for the MMS2 spacecraft; on this temporal scale, the available MMS1, MMS3, and MMS4 data were virtually identical (data not shown).

The FPI [see *Burch et al*., 2015] energy-time color spectrogram (Figure 2a) shows that the MMS spacecraft were embedded within the relatively warm plasma sheet from 18:00 UT until the shock impact at 18:36 UT. With that impact, the spacecraft went briefly into a tail lobe environment, and then for the next 35–40 min, MMS2 was in a much hotter and more dense plasma sheet environment. At about 19:10 UT, the plasma sheet began to "thin" in its north-south dimension as is commonly seen prior to substorm onsets [see *Baker et al*., 1996] and MMS2 increasingly, and somewhat sporadically, was in a tail lobe environment. All the MMS spacecraft were persistently in the tail lobe from 19:22 UT to ~19:32 UT, at which time the spacecraft were suddenly reenveloped by the expanding plasma sheet. MMS data and ground-based measures (not shown) of geomagnetic activity clearly indicated that there was a strong substorm expansion phase onset at ~19:30 UT [see *Baker et al*., 2016] As shown by Figure 1a, the MMS and VAP spacecraft were relatively well aligned in a radial sense at this time in the premidnight sector.

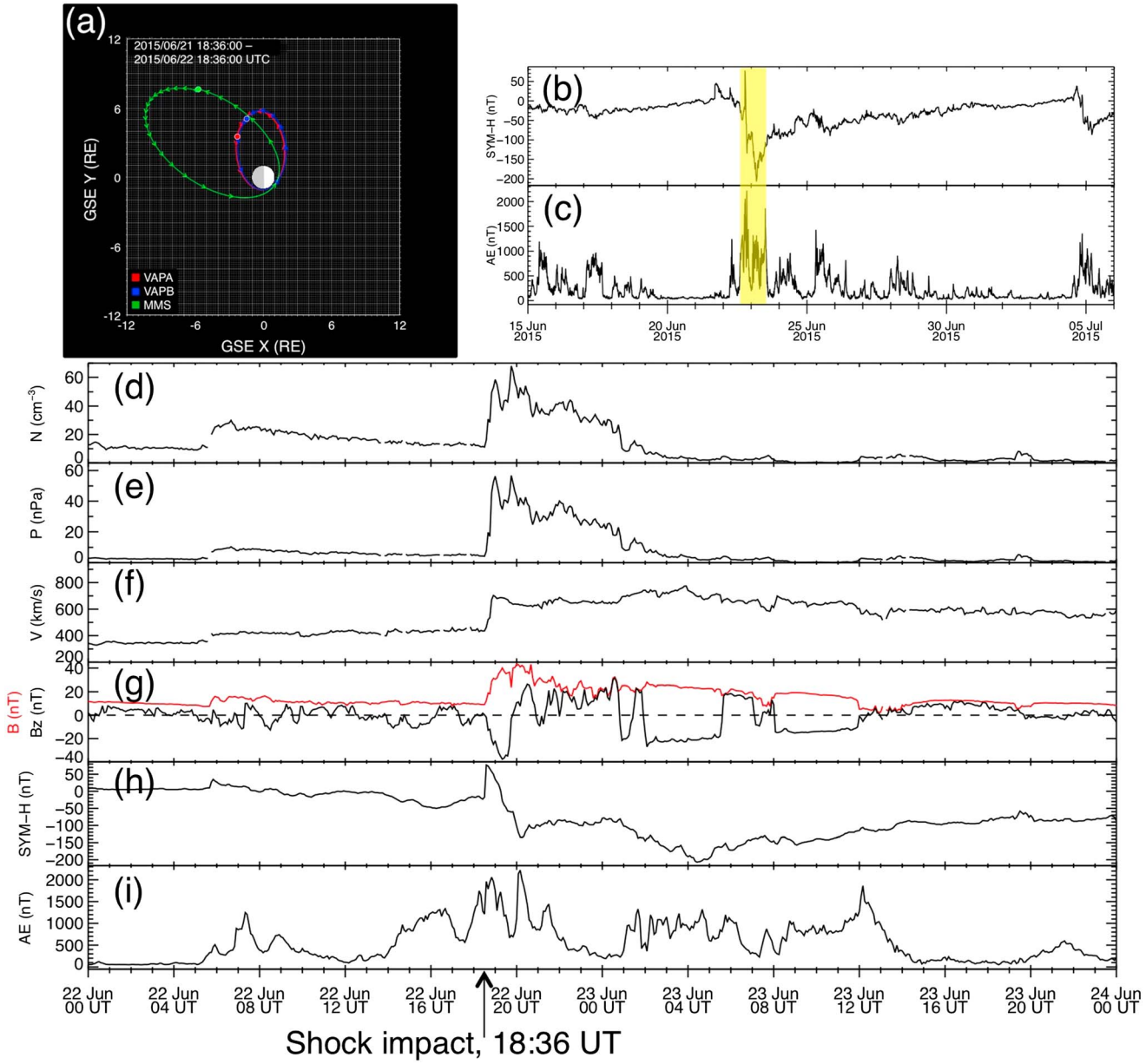

Figure 1. (a) Orbital trajectories for MMS spacecraft (green) and Van Allen Probes (red and blue) for the period of 18:36 UT on 21 June to 18:36 UT on 22 June 2015 in *x-y* projections. The colored dots in each plot show where the MMS and Van Allen Probes spacecraft were at 19:32 UT when a strong substorm onset occurred (see text). (b) *SYM-H* index and (c) *AE* index for the period of 15 June to 5 July 2015. Solar wind, IMF, and geomagnetic index data for 22–23 June 2015: (d) solar wind density, (e) solar wind dynamic pressure, (f) solar wind speed, (g) IMF $|B|$ (red) and B_z (black), (h) *SYM-H* index values, and (i) *AE* index values. A large shock wave hit Earth at 18:36 UT on 22 June as indicated by the marked time. Solar wind and IMF data (propagated to 1 AU), *SYM-H*, and *AE* are from the OMNI data set.

The FGM data [*Russell et al.*, 2014; *Torbert et al.*, 2014] from MMS2 (Figure 2b) fully support the interpretations of the last paragraph. The magnetic field signatures for 18:00–18:36 UT at MMS were those of quiet plasma sheet. At 18:36 UT, the magnetic field strength jumped up by over 120 nT in strength with the shock wave impact on the magnetosphere. From 18:40 UT to ~19:10 UT, the magnetic field was relatively weakened (characteristic of a hot, diamagnetic plasma sheet environment), and then at ~19:10 UT, the spacecraft began to enter back and forth into a high-field region characteristic of the near-tail lobe. A rapid magnetic field reconfiguration occurred at ~19:32 UT as the spacecraft was enveloped by the expanding plasma sheet associated with the substorm onset.

Figure 2c shows the energetic electron data from the EIS sensor system [*Mauk et al.*, 2014]. The energetic particles clearly track the plasma sheet-to-lobe transitions that were evident in the FPI and FGM data. In

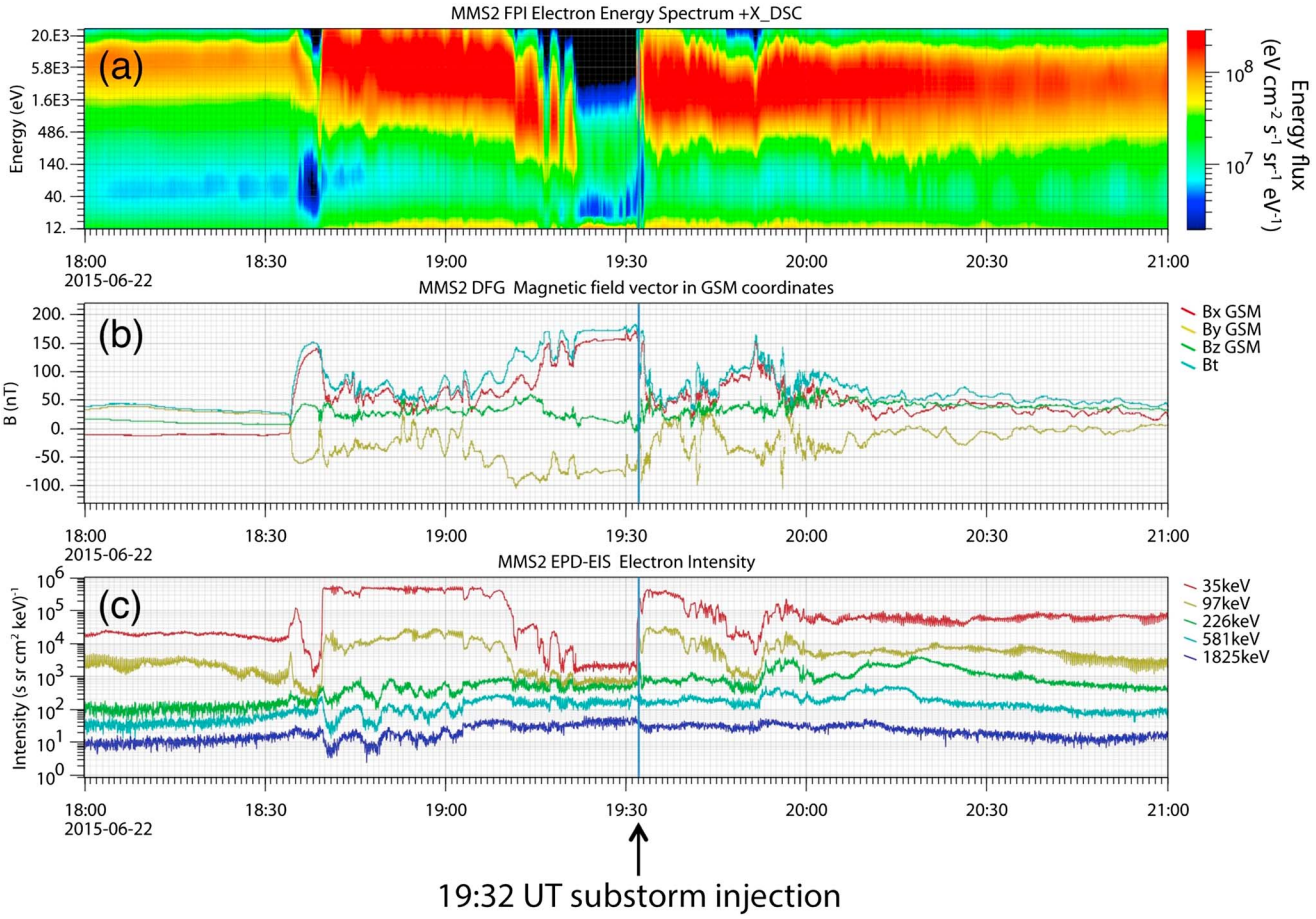

Figure 2. Data from the MMS3 spacecraft for the period of 18:00 UT to 21:00 UT on 22 June 2015. (a) Fast Plasma Investigation (FPI) electron data. (b) Flux Gate Magnetometer (FGM) magnetic field data (in GSM coordinates). (c) Energetic Ion Spectrometer (EIS) electron data. Note that the strong substorm onset indicated at 19:32 UT was obvious in both the field and particle data.

the tail lobe interval (~19:20–19:32 UT), the 30~200 keV electron fluxes were near-background values (Figure 2c). (Note that this storm interval was characterized by a weak solar energetic particle enhancement so that the EIS flux levels were already somewhat elevated during this time even before the IP shock struck the magnetosphere.) At the time of the substorm onset, electrons up to several hundreds of keV were observed to increase as the plasma sheet reenveloped the MMS spacecraft.

Figure 3 shows the detailed MMS data for the substorm onset time period. Figures 3a and 3b show the data for MMS2 for the period of 19:31 UT to 19:36 UT. The small inset shows the *x-y* locations of the MMS1, MMS2, MMS3, and MMS4 spacecraft at 19:32 UT. Figure 3a shows the magnetic field *z* component, and Figure 3b shows the proton flow speeds (*x* component) for the FPI instrument. Obviously, the reconfiguration and substorm injection event that looked so sharp in Figure 2 were highly complex when viewed with the microscopic precision of MMS in Figure 3. Multiple earthward flow bursts—some as large as 600 km/s—were seen between ~19:32 and ~19:34 UT. (Note that the derived FPI ion velocity may be up to a factor of 4 too large before ~19:32 UT due to a cold O^+ ion component and may be slightly underestimated after ~19:33 UT due to some contribution of penetrating radiation to the moment integrals.) Each of these flow bursts were accompanied by distinct, step-like increases in the local B_z component. Hence, there were multiple "dipolarization" fronts and flow bursts moving earthward during this period, consistent with the papers cited in the Introduction above. (Note that detailed EIS pitch angle plots for this period are presented in Figure S1 in the supporting information.)

Figure 3c shows a further blowup of the magnetic field data (B_z component) for the period of 19:31:30 UT to 19:32:30 UT. While for much of this period, the field data from all four MMS spacecraft were essentially

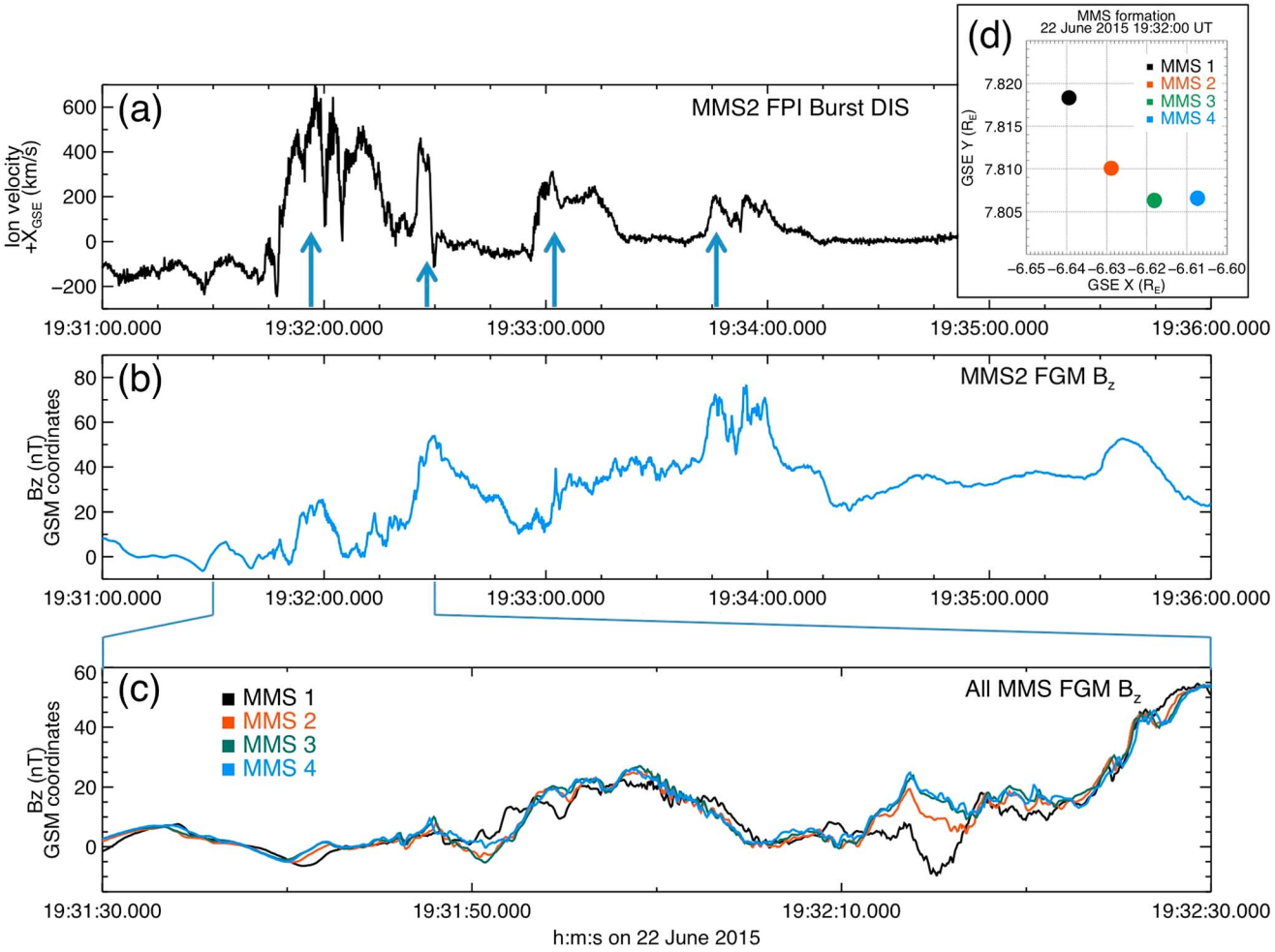

Figure 3. High-resolution (a) ion flow speeds from FPI and (b) magnetic field (B_z component) for the period of 19:31 to 19:36 UT on 22 June. (c) Even more detailed magnetic field data (19:31:30 to 19:32:30 UT) for all four MMS spacecraft (see indicated color coding). (d) Inset shows the relative spacecraft locations.

identical, at about 19:31:50 and 19:32:15 UT, there were distinct differences seen between the B_z values. As shown by the small inset, the MMS1 spacecraft was about 60 km more duskward than the MMS2 spacecraft and was also about 100 km more tailward than the MMS3 spacecraft at this time.

To find the timing and motion of two successive dipolarization front signatures, the following procedure was used. For the dipolarization front observed at MMS at 19:31:50 UT, a cross correlation on the magnitude of B_z for different spacecraft pairs was performed across the four observation time series. The velocities obtained from the cross-correlation result were compared to ensure that they were all similar (to within 30%). The velocities derived from each of the spacecraft pairs were then averaged to get a final velocity vector. Using this velocity determination, we find that the x component of the front velocity, V_x, was ~88 km/s in the earthward direction. For the front observed at MMS at 19:32:15 UT, the minimum B_z value was used to do velocity analysis, since a cross-correlation analysis was not appropriate due to the difference in trend of B_z on MMS1. For this front, a velocity component of V_x ~80 km/s was found, again in the earthward direction.

The shock wave hitting the magnetosphere at 18:36 UT and the isolated substorm that subsequently occurred at ~19:32 UT on 22 June were part of a wide and quite impressive set of responses of the outer radiation belt during this time [*Baker et al.*, 2016]. As is clear in Figure 4a, the interplanetary coronal mass ejection (ICME) impact caused a deep dropout of E~1.8 MeV electrons measured by the Relativistic Electron-Proton Telescope (REPT) sensors. The principal immediate effect of the 18:36 UT shock wave impact on the magnetosphere for electron energies $E \gtrsim 700$ keV (seen at Van Allen Probe B) was to substantially *reduce* the absolute intensities of the particles. This is shown explicitly by the detailed flux profiles in

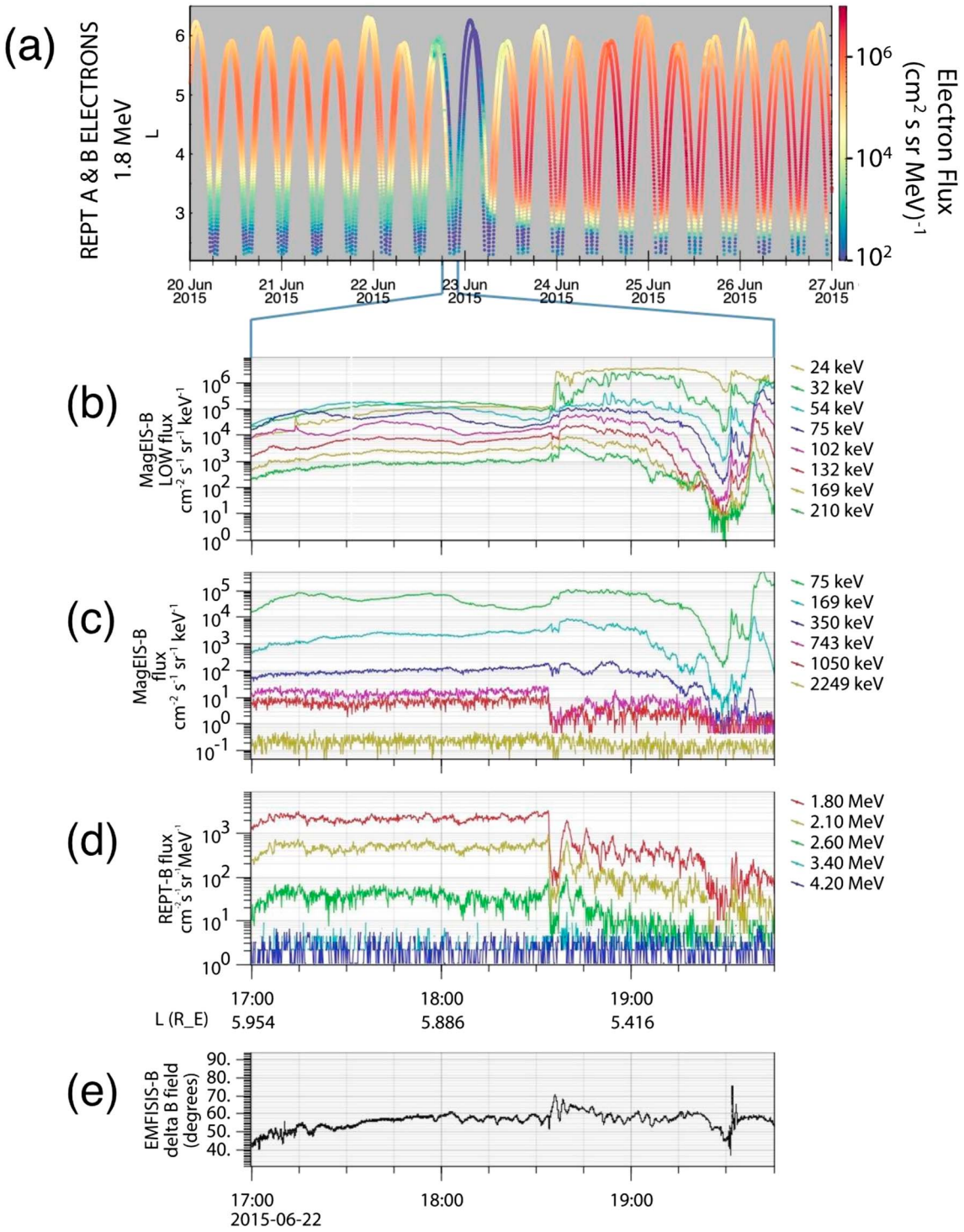

Figure 4. (a) REPT electron flux for 1.8 MeV from the broader period of 20–27 June for context. Van Allen Probe B data for the detailed period of 18:00–20:30 UT on 22 June 2015: (b) MagEIS electron fluxes from 24 to 210 keV from the low-energy unit, (c) MagEIS electron fluxes from 75 to 2249 keV from a medium-energy unit, (d) REPT electron fluxes from 1.8 MeV to 4.2 MeV, and (e) EMFISIS magnetic deflection angle data showing substorm dipolarization at 19:32 UT.

Figures 4c and 4d. These panels show the VAP B data from the Magnetic Electron Ion Spectrometer (MagEIS) [*Blake et al.*, 2013] medium-energy unit and from REPT [*Baker et al.*, 2012], respectively. As is evident in both the VAP B data (Figure 4) and in the VAP A data (Figure S2), the shock wave impact produced a deep negative pulse in the higher-energy electrons, especially those with $E > 1$ MeV. There were then "drift

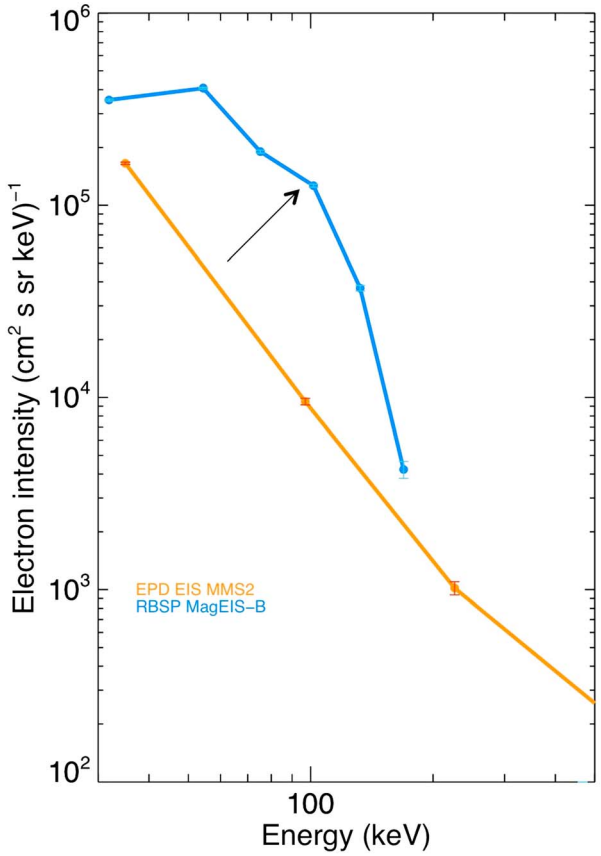

Figure 5. Comparison of the energetic electron energy spectrum measured by MMS2 EIS (gold color) averaged over 19:32–19:33 UT and the subsequent spectrum measured by VAP B MagEIS (blue color) averaged over ~19:39–19:40 UT. A large flux increase was seen over this time, up to over a hundred keV. The MagEIS values are background corrected, and the error bars are plotted from error given in the data files. The EIS error bars are estimated based on counting statistics.

echo" returns of the depletion pulse that went on for the next hour or so, especially at the VAP B location. In contrast, lower-energy electrons with $20 \lesssim E \lesssim 300$ keV were *enhanced* in flux levels following the shock impact (Figure 4b). This is consistent with the analyses presented by *Turner et al.* [2012] and *Boyd et al.* [2014] using phase space density analyses from VAP for other shock impact events.

As shown by the Van Allen Probe B data (Figure 4e) the substorm onset at 19:32 UT produced a strong spike in the Electric and Magnetic Field Instrument Suite and Integrated Science magnetic field angle and also caused a recovery of 20 keV~200 keV electron fluxes to pregrowth phase levels (Figure 4b). Thus, it was seen that the low-to-moderate energy electrons at VAP B gradually diminished in absolute intensity as the magnetosphere developed a more stretched and tail-like field configuration from ~19:00 UT to 19:32 UT. This was the precise counterpart to the plasma sheet thinning observed at MMS (as shown in Figure 2a above) and was a global signature of the substorm growth phase [e.g., *Baker et al.*, 1996].

Following the 19:32 UT flux recovery and magnetic field pulse at VAP B there was a strong injection of freshly accelerated electrons with energies up to several hundreds of keV, indicating an intense building of the ring current population very immediately. This pulse of electrons (shown by the bold arrows in Figure 4) was somewhat dispersive in energy with the highest energies arriving at VAP B at ~19:38 UT. The lowest-energy electrons (~24 keV) observed by MagEIS were delayed in arrival until somewhat after 19:40 UT. We interpret this pulse (19:38–19:40 UT) of electrons to be the transported counterpart of the dipolarization front-related electrons observed at ~19:32 UT by MMS sensors.

While undergoing the earthward transport into stronger magnetic field regions, we would expect to observe an enhanced electron energy spectrum for the transported population. Figure 5 shows that this indeed was the case. The yellow curve in Figure 5 shows the electron energy spectrum measured by the MMS/EIS sensors from 19:32 to 19:33 UT. The blue curve in Figure 5 is the peak energy spectrum measured by the Van Allen Probe B sensors (MagEIS) during the interval of 19:39–19:40 UT. A substantial increase in flux magnitude is evident from 50 to 150 keV. We attribute this to the earthward transport and injection from the MMS to the VAP locations. This presumably is due primarily to earthward motion of an electromagnetic pulse rather than material transport of an entire coherent population of electrons [see *Li et al.*, 1998].

4. Discussion

The combination of Magnetospheric Multiscale and Van Allen Probes measurements has permitted a new application of the telescope-microscope technique employed successfully in earlier studies. The precise timing of dipolarization front motion over the several MMS spacecraft allows us to do accurate timing during

a sharp substorm expansion phase onset. The corresponding observations from the Van Allen Probes spacecraft during the substorm expansion phase onset allow us to detect later the injected particle population several Earth radii away from the MMS spacecraft. The timing of the injection front motion over nearly 5 R_E of separation permits estimation of boundary motion seen both locally by the MMS constellation elements and on the mesoscale by the Van Allen Probe B spacecraft.

A dipolarization front moving at ~88 km/s in passing the MMS spacecraft constellation would be expected to reach the Van Allen Probe B location at ~19:38 UT. This follows from the MMS constellation being (see Figure 1) at $r_{x\text{-GSE}}$~10.2 R_E and VAP B being at $r_{x\text{-GSE}}$~4.5 R_E: a difference of ~5.7 $R_E = 36320$ km. For a front moving at the measured speed, this would lead to an expected arrival time difference of $\left(\frac{36,320}{88}\right)$ ~410 s. Thus, we would expect arrival at VAP B of (19:32 UT + 6.8 min)~19:38:48 UT (consistent with the actual observations). This also indicates that the earthward propagating front had not slowed significantly in moving from the MMS to VAP B locations.

Our velocity analysis agrees well with the timing we find from the observational data of both distinctive MMS fronts, occurring between 19:31:50 and 19:32:15 UT. The inner magnetosphere injection could have resulted from either of the dipolarization front features, even if no significant flow braking [i.e., *Sergeev et al*., 1998] took place between the two observations. However, the measured flows were much higher than the 24 km/s reported by *Reeves et al*. [1996]. These results point out the importance of obtaining more observations of injection signatures and flow-braking events in the coming MMS tail phases.

On a more global scale, the event under study here on 22 June 2015 occurred during a powerful geomagnetic storm (*SYM-H* = −207 nT) that was driven by a well-observed coronal mass ejection. From a highly energetic electron point of view (i.e., $E \gtrsim 1$ MeV), the entire outer belt was reduced in electron intensity by a factor of 10 to 100 within at most a few hours upon the shock wave hitting Earth's vicinity. It took 1 to nearly 3 days (depending on energy) for the relativistic electrons to recover. On the other hand, we have shown that ring current electrons from ~20 keV to ~300 keV were suddenly (and impressively) enhanced in absolute intensity by the shock impact. Electrons in this low-to-moderate energy range were further accelerated by the 19:32 UT substorm onset. Clearly, these electrons formed the "seed" population [see *Jaynes et al*., 2015] that would eventually reconstitute the relativistic electron outer belt population over the next 1–3 days. As noted by *Turner et al*. [2012] and *Boyd et al*. [2014], only electrons with energies below a few hundreds of keV have sufficient phase space density in the near-Earth plasma sheet to act as the seed population. Electrons at higher energies must be produced by subsequent other processes as discussed in *Jaynes et al*. [2015, and references therein].

In summary, this event has allowed us to see the solar storm that produced the ICME and shock, to observe the radiation belt depletion, and to measure the substorm injection front in great detail that ultimately supplied the seed particles for restoration of the outer radiation belt. This is the multiscale observation capability that has long been needed to help complete our understanding of the global Sun-Earth system in all of its many manifestations.

Acknowledgments
This work was supported by funding from the MMS mission, under NASA contract NNG04EB99C. MMS data are available at https://lasp.colorado.edu/mms/sdc/ or by request for dates earlier than 1 September 2015. Van Allen Probes data and solar wind OMNI data from ACE and Wind are available via the Space Physics Data Facility at http://cdaweb.gsfc.nasa.gov/istp_public/.

References

Acuña, M. H., K. W. Ogilvie, D. N. Baker, S. A. Curtis, D. H. Fairfield, and W. H. Mish (1995), The Global Geospace Science program and its investigations, *Space Sci. Rev.*, *71*, 5–21.

Angelopoulos, V., W. Baumjohann, C. F. Kennel, F. V. Coroniti, M. G. Kivelson, R. Pellat, R. J. Walker, H. Luhr, and G. Paschmann (1992), Bursty bulk flows in the inner central plasma sheet, *J. Geophys. Res.*, *97*(A4), 4027–4039, doi:10.1029/91JA02701.

Baker, D. N., T. I. Pulkkinen, V. Angelopoulos, W. Baumjohann, and R. L. McPherron (1996), The neutral line model of substorms: Past results and present view, *J. Geophys. Res.*, *101*, 12,995–13,010, doi:10.1029/95JA03753.

Baker, D. N., R. E. Ergun, J. L. Burch, J.-M. Jahn, P. W. Daly, R. Friedel, G. D. Reeves, T. A. Fritz, and D. G. Mitchell (2002), A telescopic and microscopic view of a magnetospheric substorm on 31 March 2001, *Geophys. Res. Lett.*, *29*(18), 1862, doi:10.1029/2001GL014491.

Baker, D. N., et al. (2012), The Relativistic Electron-Proton Telescope (REPT) instrument on board the Radiation Belt Storm Probes (RBSP) spacecraft: Characterization of Earth's radiation belt high-energy particle populations, *Space Sci. Rev.*, *170*(1), 337–381, doi:10.1007/s11214-012-9950-9.

Baker, D. N., et al. (2016), New results for high-energy protons and electrons in the inner Van Allen belt region Symposium ST2.5, EGU Meeting, Vienna, Austria, 20 April 2016.

Birn, J., M. F. Thomsen, J. E. Borovsky, G. D. Reeves, D. J. McComas, R. D. Belian, and M. Hesse (1998), Substorm electron injections: Geosynchronous observations and test particle simulations, *J. Geophys. Res.*, *103*(A5), 9235–9248, doi:10.1029/97JA02635.

Birn, J., A. V. Artemyev, D. N. Baker, M. Echim, M. Hoshino, and L. M. Zelenyi (2012), Particle acceleration in the magnetotail and aurora, *Space Sci. Rev.*, *173*, doi:10.1007/s11214-012-9874-4.

Blake, J. B., et al. (2013), The *Magnetic Electron Ion Spectrometer* (MagEIS) instruments aboard the Radiation Belt Storm Probes (RBSP) spacecraft, *Space Sci. Rev.*, *179*(1), 383–421, doi:10.1007/s11214-013-9991-8.

Boyd, A. J., H. E. Spence, S. G. Claudepierre, J. F. Fennell, J. B. Blake, D. N. Baker, G. D. Reeves, and D. L. Turner (2014), Quantifying the radiation belt seed population in the March 17, 2013 electron acceleration event, *Geophys. Res. Lett.*, *41*, 2275–2281, doi:10.1002/2014GL059626.

Burch, J. L., T. E. Moore, R. B. Torbert, and B. L. Giles (2015), Magnetospheric Multiscale overview and science objectives, *Space Sci. Rev.*, *199*(1), 5–21, doi:10.1007/s11214-015-9164-9,2015.

Burch, J. L., et al. (2016) Electron-scale measurements of magnetic reconnection in space, *Science*, in press, doi:10.1126/science.aaf2939.

Gabrielse, C., V. Angelopoulos, A. Runov, and D. L. Turner (2014), Statistical characteristics of particle injections throughout the equatorial magnetotail, *J. Geophys. Res. Space Physics*, *119*, 2512–2535, doi:10.1002/2013JA019638.

Jaynes, A. N., et al. (2015), Source and seed populations for relativistic electrons: Their roles in radiation belt changes, *J. Geophys. Res. Space Physics*, *120*, 7240–7454, doi:10.1002/2015JA021234.

Li, X., D. N. Baker, M. Temerin, G. D. Reeves, and R. D. Belian (1998), Simulation of dispersionless injections and drift echoes of energetic electrons associated with substorms, *Geophys. Res. Lett.*, *25*(20), 3763–3766, doi:10.1029/1998GL900001.

Liu, J., V. Angelopoulos, X.-Z. Zhou, and A. Runov (2014), Magnetic flux transport by dipolarizing flux bundles, *J. Geophys. Res. Space Physics*, *119*, 909–926, doi:10.1002/2013JA019395.

Liu, J., V. Angelopoulos, X.-J. Zhang, D. L. Turner, C. Gabrielse, A. Runov, J. Li, H. O. Funsten, and H. E. Spence (2016), Dipolarizing flux bundles in the cis-geosynchronous magnetosphere: Relationship between electric fields and energetic particle injections, *J. Geophys. Res. Space Physics*, *121*, 1362–1376, doi:10.1002/2015JA021691.

Mauk, B. H., N. J. Fox, S. G. Kanekal, R. L. Kessel, D. G. Sibeck, and A. Ukhorsky (2012), Science objectives and rationale for the Radiation Belt Storm Probes mission, *Space Sci. Rev.*, *179*(1), 1362–1357, doi:10.1007/s11214-012-9908-y.

Mauk, B. H., et al. (2014), The Energetic Particle Detector (EPD) investigation and the Energetic Ion Spectrometer (EIS) for the Magnetospheric Multiscale (MMS) mission, *Space Sci. Rev.*, doi:10.1007/s11214-014-0055-5.

National Research Council (2013), *Solar and Space Physics: A Science for a Technological Society*, The National Academies Press, Washington, D. C., doi:10.17226/13060.

Reeves, G. D., M. G. Henderson, P. S. McLachlan, R. D. Belian, R. H. W. Freidel, and A. Korth (1996), Radial propagation of substorm injections, in *the Proc. of Substorms*, vol. 3, edited by E. J. Rolfe and B. Kaldeich, pp. 579–584, ESA, Paris SP-339.

Runov, A., V. Angelopoulos, X.-Z. Zhou, X. -J. Zhang, S. Li, F. Plaschke, and J. Bonnell (2011), A THEMIS multicase study of dipolarization fronts in the magnetotail plasma sheet, *J. Geophys. Res.*, *116*, A05216, doi:10.1029/2010JA016316.

Russell, C. T., et al. (2014), The Magnetospheric Multiscale magnetometers, *Space Sci. Rev.*, *199*(1), 189–256, doi:10.1007/s11214-014-0057-3.

Sergeev, V. A., M. A. Shukhtina, R. Rasinkangas, A. Korth, G. D. Reeves, H. J. Singer, M. F. Thomsen, and L. I. Vagina (1998), Event study of deep energetic particle injections during substorm, *J. Geophys. Res.*, *103*(A5), 9217–9234, doi:10.1029/97JA03686.

Torbert, R. B., et al. (2014), The FIELDS instrument suite on MMS: Scientific objectives, measurements and data products, *Space Sci. Rev.*, *199*(1), 105–135, doi:10.1007/s11214-014-0109-8.

Turner, D. L., V. Angelopoulos, Y. Shprits, A. Kellerman, P. Cruce, and D. Larson (2012), Radial distributions of equatorial phase space density for outer radiation belt electrons, *Geophys. Res. Lett.*, *39*, L09101, doi:10.1029/2012GL051722.